

DRA



SRB NOZZLE EROSION RELATED FLOW ANALYSIS

Contract No. NAS8-35767

FINAL REPORT

(NASA-CR-170961) THE SRB NOZZLE EROSION
RELATED FLOW ANALYSIS Final Report
(Continuum, Inc.) 15 p HC A02/MF A01

N84-16251

CSCI 21H

Unclas

G3/20 00557

Prepared For:

National Aeronautics and Space Administration
George C. Marshall Space Flight Center
Marshall Space Flight Center, Alabama

Prepared By:

CONTINUUM, INC.
Robert J. Prozan
4715 University Drive, Suite 118
Huntsville, AL 35805

(205) 837-9310

December 19, 1983

FOREWARD AND SUMMARY

The effort reported in this document was performed by Continuum, Inc., Huntsville, Alabama in support of the National Aeronautics and Space Administration, George C. Marshall Space Flight Center, Marshall Space Flight Center, Alabama. This document is the final report required under Contract No. NAS8-35767 entitled "SRB Nozzle Erosion Related Flow Analysis". The technical direction for this study was supplied by Dr. G. A. Wilhold (ED31) of MSFC.

The study was performed to define the SRB nozzle throat flow field, and to investigate one possible mechanism for the severe erosion which occurred on a recent flight. The flow field in the vicinity of the eroded area was not found to be exceptional, and the presence of a notch or scored area near the imbedded region nose did not appear to produce sufficient flow fluctuations to exacerbate the erosion characteristics of the throat liner. An interesting fluctuating mechanism was found in the imbedded cavity, but that mechanism (while of possible importance for erosion of the seal region) did not seem to adversely affect the region of concern.

On the basis of this analysis, the conclusion can be drawn that the anomalous erosion did not result from a single mechanical defect (pit, or gouge) since the flow fluctuations which result seem insufficient to induce a repetitive pattern downstream. It further appears that the erosion pattern exhibited did not result from a steady flow phenomena in the throat region. This does not rule out acoustic phenomena or severe start-up transients. To investigate the latter phenomena was considerably beyond the scope of this quick response effort.

INTRODUCTION

The severe erosion pattern discovered in the SRB throat region after a recent flight was cause for concern that, unless understood and corrected, a burn through might occur on a subsequent flight. Discussions with cognizant NASA/MSFC personnel indicated that there were no apparent anomalies in the flight behavior of the engine which might explain the massive erosion which actually occurred. The consensus was that a mechanical/materials/processing problem was the underlying cause. Nevertheless, other phenomena which might induce such an erosive pattern had to be investigated.

Details of the flow field in the vicinity of the eroded area were not available due to the previous limitations of computational/numerical modeling. The general behavior of transonic flow fields in conventional nozzle throat regions is reasonably well understood. The SRB has a very large ratio of entrance radius of curvature to throat radius which lends itself quite well to simplified series expansion techniques such as are currently in use in the standard JANNAF performance model. These techniques, however, do not adequately model the complex geometry of the imbedded nozzle, nor do they treat the flow patterns caused by burning surfaces in the proximity of the nozzle entrance.

The introduction, by Continuum, Inc. of the variational methodology, (1,2) permits the analysis of extremely complex geometric domains with a very efficient numerical algorithm for unsteady elliptic (or spatially hyperbolic) flows. These techniques were employed in the solution of the problems chosen in order to explore possible erosion mechanisms.

The first task was to produce a numerical analysis of the entire region to ascertain whether or not a primary erosive mechanism might result from the contorted flow field near the nozzle nose. The question also arose whether a single mechanical defect in the nose region could induce the repeated erosive pattern which the flight nozzle exhibited. If so, a single gouge or pit in the nozzle liner surface could explain the repetitious erosion pattern. The second task was to perform an analysis of subsonic flow over a postulated cavity to determine the severity of the fluctuations downstream and the possibility of the generation of a repeated pattern from a single flaw.



TECHNICAL DISCUSSION

Three flow field situations were analyzed using operating conditions established by cognizant NASA/MSFC personnel:

- o Case 1: The entrance and transonic region of the SRB very early in the burn when neither the imbedded region nor the port region grain have regressed substantially. The inviscid analysis was performed on the Continuum CM-1000 workstation.
- o Case 2: The entrance and transonic region of the SRB at approximately 90 seconds into the burn when the imbedded region grain had completely burned and the port had regressed to the point that it could be considered to occupy the entire case diameter. The inviscid analysis was performed on the NASA CM-1000 workstation.
- o Case 3: The subsonic flow past a square notch and the resultant downstream disturbances. This viscous flow analysis was performed on the ARC 7600.

Figure 1 illustrates the grid distribution for Case 1. The blue lines are the internal field discretization lines while the red lines indicate solid walls (in this context the centerline is a solid wall). Inlets are indicated by green lines. Two different inlet situations apply: (1) the port flow which is a permeable boundary; and (2) the grain surface which injects mass, momentum and energy into the field, but whose injection rate is specified by a burn rate expression as follows:

$$r = b (\rho)^n e^{\pi_k (1-n) (T-T_f)}$$

where r is the mass injection rate, b is a constant, ρ is the local surface pressure, T is the local surface temperature, T_f is the flame temperature, n is the burn rate exponent controlling pressure dependence and π_k is a temperature dependence coefficient. For this analysis, n was taken to be $1/2$ while π_k was taken to be $.002$.



The port flow distribution input as a permeable boundary was calculated from the basic flux data supplied by NASA/MSFC, but was distributed laterally according to the analysis of reference 3. The reference analysis indicates that the mass is injected normal to the stream, and that the axial velocity at the grain surface is zero. The exit from the port is, therefore, assumed to have this distribution. Due to the coarse grid used in the imbedded region the normal velocity is not assumed to be zero at the grain surface. The validity of this assumption obviously correlates to grid size and it is reasonable to allow tangential flow adjacent to the surface for coarse grids.

Figure 2 gives the velocity and Mach number distribution throughout the computational domain. The spike in the $M = .2$ contour adjacent to the inlet permeable boundary indicates a mismatch between the inlet specification and the downstream controlling transonic flow pattern. It is a property of subsonic flow that information can communicate upstream. Since the reference 3 analysis does not account for this, some mismatch is inevitable. It is striking, however, how quickly the flow field regains a conventional transonic behavior.

The solution was run until the field converged to a tolerance of 1 ft./sec. on velocity. The behavior of the Mach contours adjacent to the outlet are generally typical of Mach contours for flow exiting a throat circle and being slightly recompressed by the discontinuity in the derivative of the wall slope where the diffuser contour attaches to the throat circle. The influence of the outlet may also alter the Mach contours near the exit. The diffuser was not included in the analysis since in supersonic flow no backward communication is possible. No unusual or unexpected phenomena occurred in the analysis which would justify the conclusion that the basic flow structure in Case 1 contributed to the anomalous erosion pattern.

The Case 2 computational domain is given in Figure 3. The computational domain actually extends a considerable distance back towards the head end of the motor, but is not shown in the figure. For this analysis the port flow was assumed to be laterally constant since there is a long entrance in which the flow can return to a one-dimensional character. As can be seen in this figure, the imbedded region grain has also burned back to the case so that no burning surface is included in the computation. A somewhat finer grid density was used in this case. Once again, the solid walls are red while the internal element discretization is blue. Since the inlet is further upstream it is not shown on this figure.

Figure 4 gives the velocity and Mach number distributions for this flow situation. As in Case 1, the results in the transonic region do not indicate any unusual behavior. In fact, the entrance flow field is remarkably like a source flow. In the imbedded region cavity, however, a slow filling and emptying of the cavity was noticed. Since a true transient initial condition was not employed, there exists the possibility that the behavior is due to initial conditions. It is also reasonable to conclude that the cavity will, in actuality, respond in this fashion. Close-up views of the flow pattern near the nose of the entrance contour are presented versus time in Figure 5. Apparently the phenomena is of such low energy that it does not disrupt the entrance field. This phenomena could be of importance in determining burn back patterns and seal life, but does not appear to be of importance to the erosion question.

Figure 6 (Case 3) shows the computational domain used to assess the behavior of the entrance flow in the presence of a single notch in the nozzle wall. Previous studies of the flow fields resulting from flow over a cavity indicate that sharp slots (rather than rounded pits) create the greatest disturbance. The configuration chosen for analysis corresponds to a severe case of mechanical damage and, at the same time, corresponds to the type of defect which would most severely disrupt the flow field downstream. Figure 7 shows the velocity distribution and pressure distribution which resulted from a slot of these dimensions. The flow pattern labeled (A) is the top portion of the cavity which has fluctuating velocity components in the vertical direction, while (B) includes the freestream shear layer on top of the cavity and (C) is the velocity distribution one cavity width downstream. The flow shows a definite unsteady (or quasi-steady) behavior which is typical of subsonic flows over cavities. The flow pattern which results is a function of the local Mach number, shape of the cavity, and cavity size. Our computational experience in cavity flows encompasses several cavity calculations at various subsonic and supersonic Mach numbers. The pressure fluctuations of approximately 1% of freestream are typical of this type of unsteady flow field. The fluctuating velocity component perpendicular to the wall downstream of the cavity is of the order of 20 ft./sec. Additional plots at various times which clearly reveal the unsteady nature of the phenomena can be produced if desired. This information was informally conveyed to the NASA/MSFC personnel during the SRB erosion review. It is our judgement, based on previous experience and on this calculation, that a single mechanical defect of this type would not induce the repeated and severe erosion witnessed in the flight article.

CONCLUSIONS

Based on the results of this study, Continuum, Inc. has eliminated the following as potential causes of the observed erosion pattern in the flight motor:

- o The steady operating flow field is not unlike that found in conventional nozzle entrances; the erosion pattern cannot be caused by the transonic steady flow field.

- o The repeated pattern was not a result of a single upstream defect or pit in the nozzle.

In addition, it should also be pointed out that this analysis does not rule out other more complex phenomena as contributors to the erosion mechanism. Acoustic phenomena and start-up transient anomalies are possible candidates which should be investigated. It should also be noted that the analysis indicates that there may be a very low frequency resonance in the imbedded region cavity which, although not a contributor to the erosion problem under investigation, may be of significance in the cavity burn back and on the gimbaled nozzle seal life.

REFERENCES

1. Prozan, R.J., "A Variational Principle for Compressible Fluid Mechanics (Discussion of the One-Dimensional Theory)", NASA CR 3526, April 1982
2. Prozan, R.J., " A Variational Principle for Compressible Fluid Mechanics (Discussion of the Multi-Dimensional Theory)", NASA CR 3614, October 1982
3. Dunlap, R., et.al. "Flowfield in the Combustion Chamber of a Solid Propellant Rocket Motor", Vol 12, No. 10, 1974

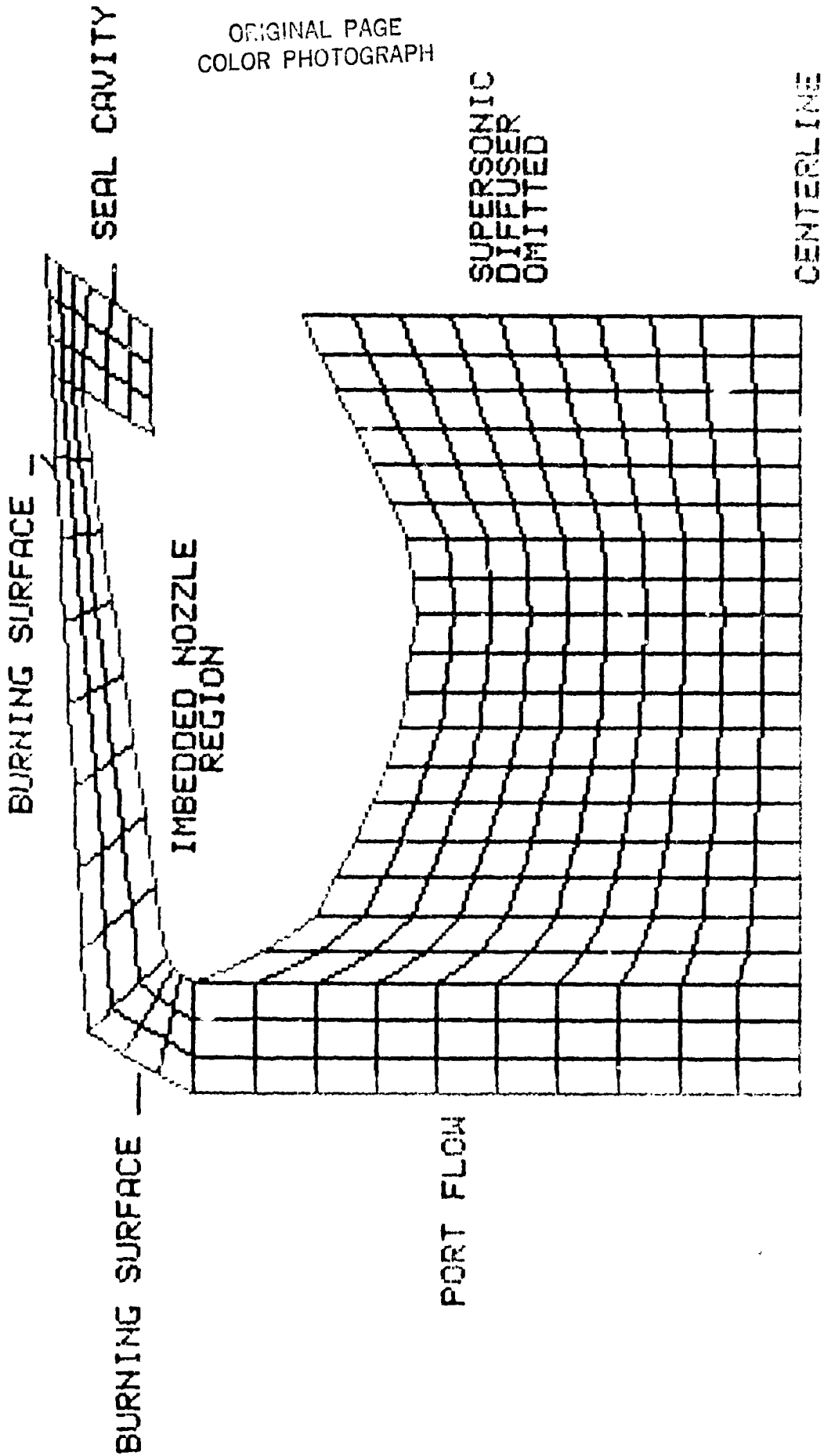
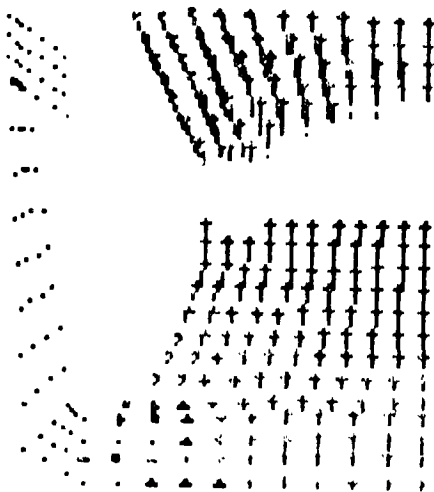


FIGURE 1 GRID DEFINITION (EARLY IN THE BURND)



UPPER LEFT	LOWER LEFT	LOWER RIGHT
FLOW VECTOR AT STEP 5600 ELAPSED TIME 0.265941	MACH NUMBER AT STEP 5600 ELAPSED TIME 0.265941	MACH NUMBER AT STEP 5600 ELAPSED TIME 0.265941
5000.	1.	2.
4000.	0.8	1.8
3000.	0.6	1.6
2000.	0.4	1.4
1000.	0.2	1.2
0.	0.	1.



ORIGINAL PAGE
COLOR PHOTOGRAPH



FIGURE 2 FLOW DIRECTION AND MAGNITUDE (FT/SEC)
AND MACH CONTOURS FOR CASE 1

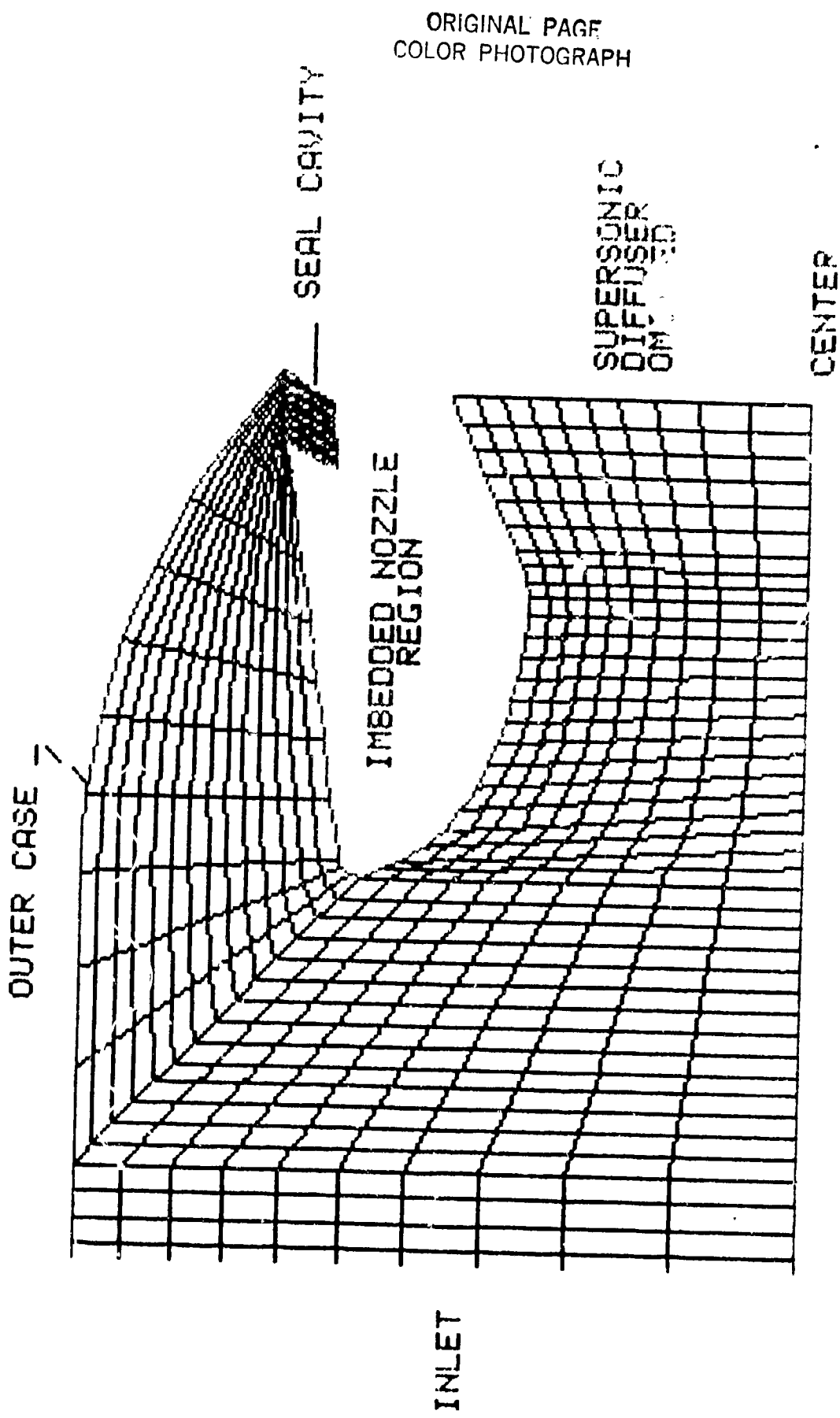


FIGURE 3 GRID DEFINITION FOR CASE 2
(90 DEGREES INTO BURND)



ORIGINAL PAGE
 COLOR PHOTOGRAPH

UPPER LEFT	LOWER LEFT	LOWER RIGHT
FLOW VECTOR AT STEP 4000 ELAPSED TIME 0.9837E-02	MACH NUMBER AT STEP 4000 ELAPSED TIME 0.9837E-02	MACH NUMBER AT STEP 4000 ELAPSED TIME 0.9837E-02
5000.	1.	2.
4000.	0.8	1.8
3000.	0.6	1.6
2000.	0.4	1.4
1000.	0.2	1.2
0.	0.	1.

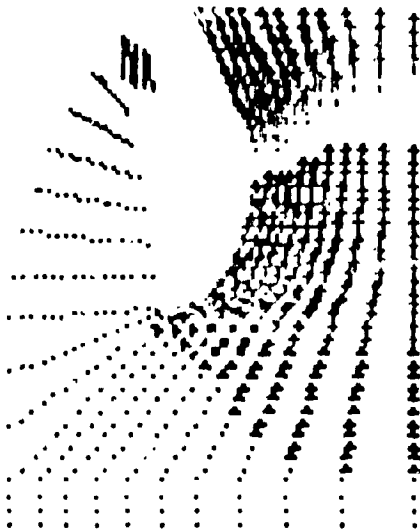
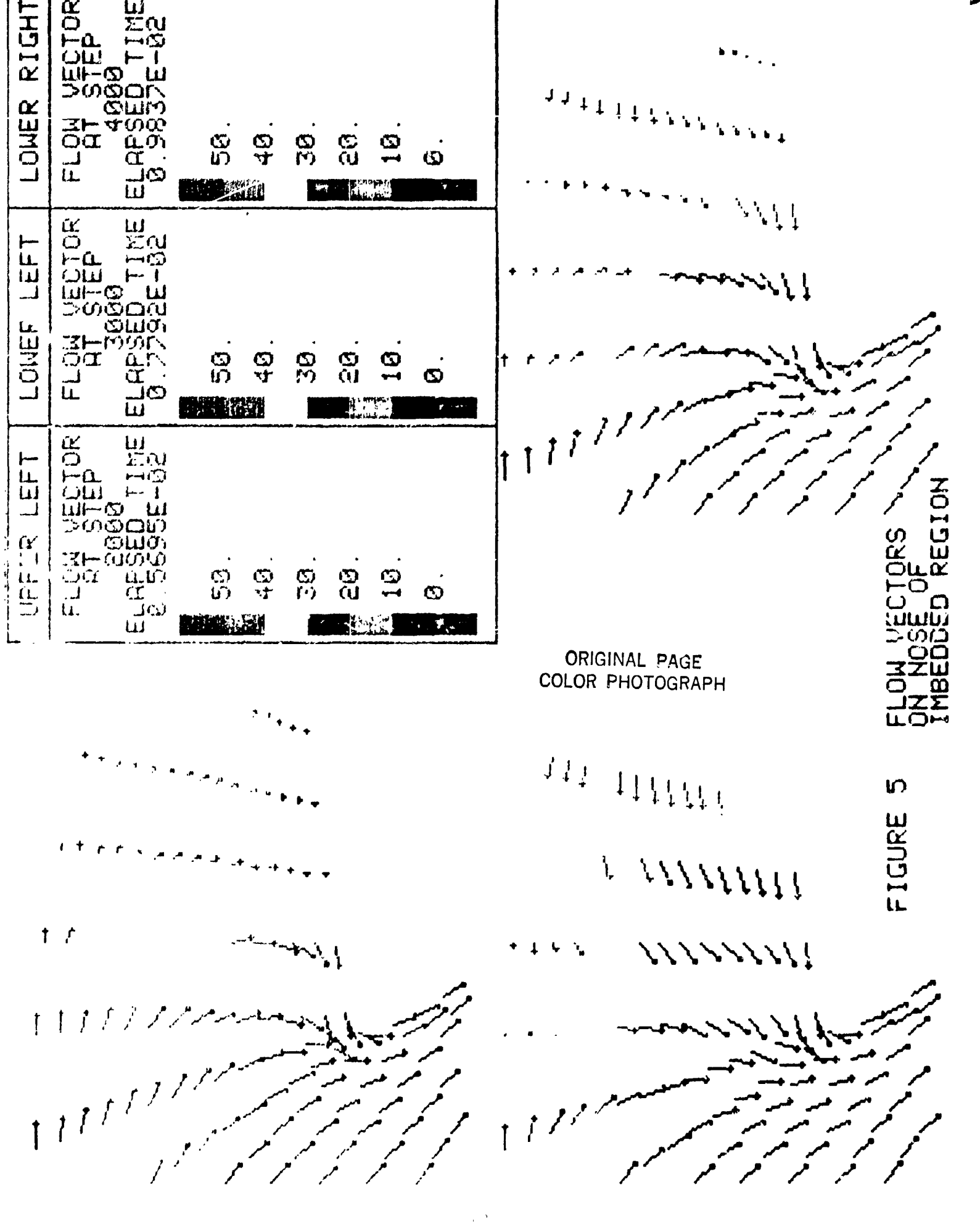


FIGURE 4 FLOW DIRECTION AND MAGNITUDE (FT/SEC) AND MACH CONTOURS FOR CASE 2

UPPER LEFT	LOWER LEFT	LOWER RIGHT
FLOW VECTOR AT STEP 3000 ELAPSED TIME 0.9595E-02	FLOW VECTOR AT STEP 3000 ELAPSED TIME 0.7792E-02	FLOW VECTOR AT STEP 4000 ELAPSED TIME 0.9837E-02
50. 40. 30. 20. 10. 0.	50. 40. 30. 20. 10. 0.	50. 40. 30. 20. 10. 0.

ORIGINAL PAGE
 COLOR PHOTOGRAPH

FIGURE 5 FLOW VECTORS
 ON NOSE OF
 IMBEDDED REGION



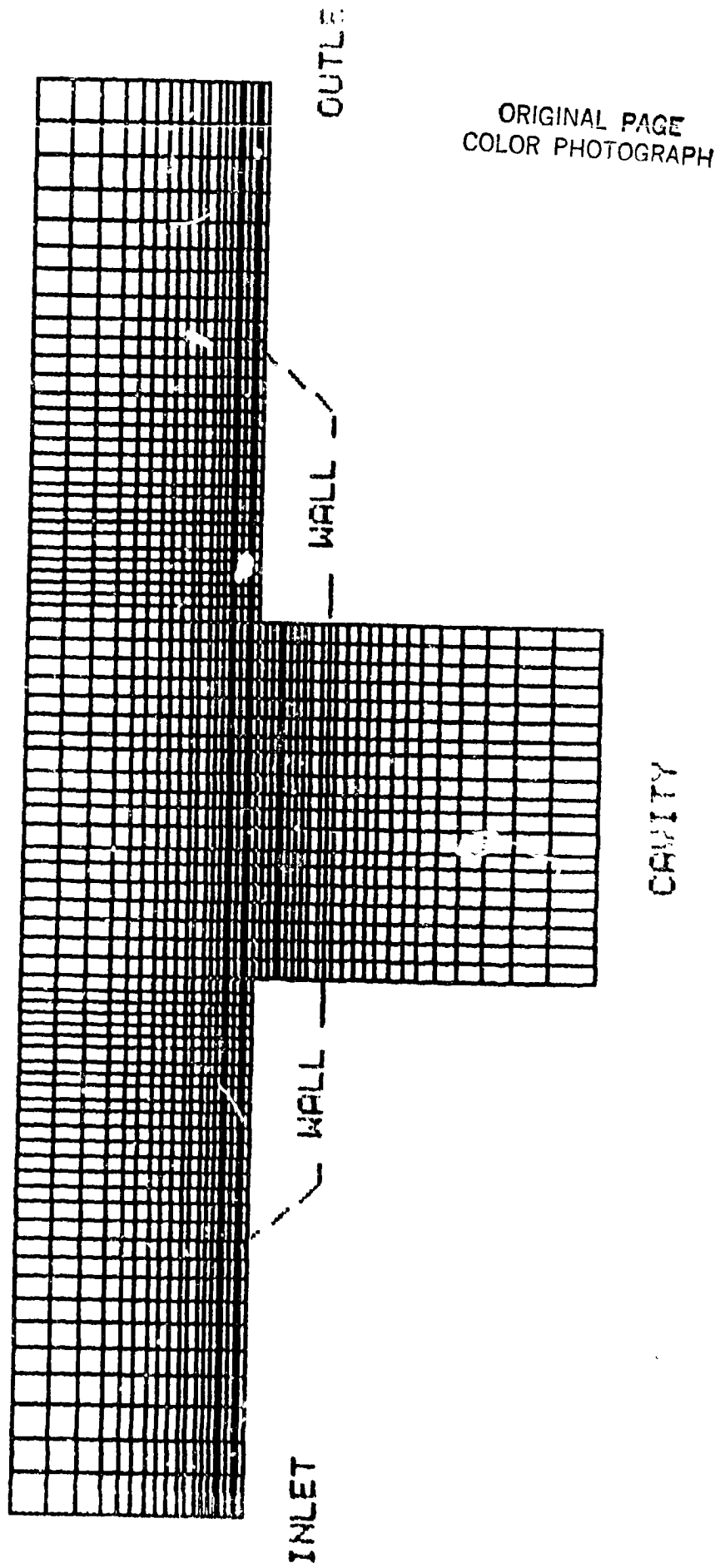
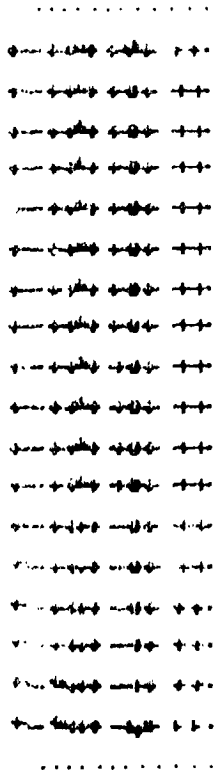


FIGURE 6 CASE 3 GRID DISTRIBUTION FOR CAVITY ANALYSIS



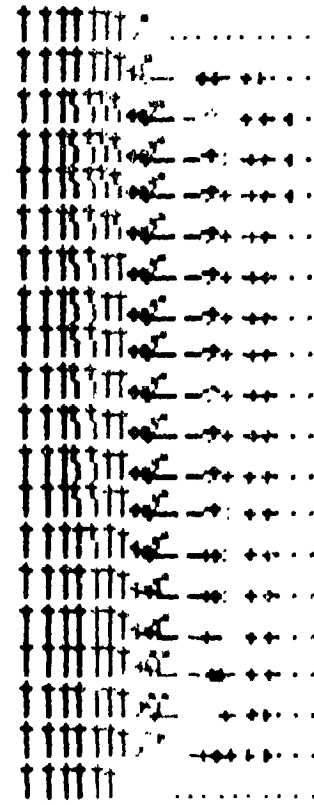
UPPER LEFT	LOWER LEFT	LOWER RIGHT
FLOW VECTOR AT STEP ELAPSED TIME 1.8951E-3	FLOW VECTOR AT STEP ELAPSED TIME 1.8951E-3	FLOW VECTOR AT STEP ELAPSED TIME 1.8951E-3
1000	1000	1000
800	800	800
600	600	600
400	400	400
200	200	200
0	0	0

A



ORIGINAL PAGE
COLOR PHOTOGRAPH

B



C

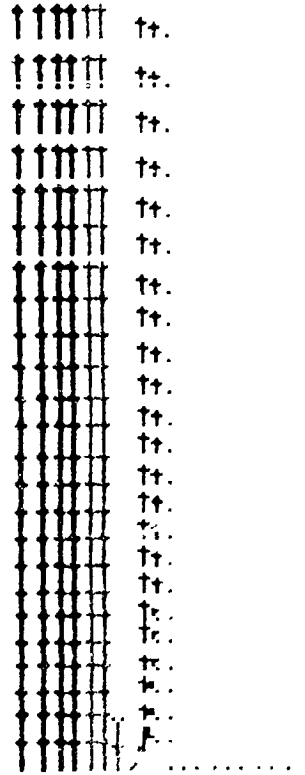


FIGURE 7 CAVITY VELOCITY COMPONENTS
CASE 3